


Interference mechanism of cations on transport of lithium and magnesium inside COF nanofiltration membranes

Decai Liao, Zhaoqin Xu, Mingjie Wei & Yong Wang


To cite this article: Decai Liao, Zhaoqin Xu, Mingjie Wei & Yong Wang (2022) Interference mechanism of cations on transport of lithium and magnesium inside COF nanofiltration membranes, Molecular Simulation, 48:15, 1369-1377, DOI: [10.1080/08927022.2022.2094372](https://doi.org/10.1080/08927022.2022.2094372)

To link to this article: <https://doi.org/10.1080/08927022.2022.2094372>

 View supplementary material [↗](#)

 Published online: 01 Jul 2022.

 Submit your article to this journal [↗](#)

 Article views: 223

 View related articles [↗](#)

 View Crossmark data [↗](#)



Interference mechanism of cations on transport of lithium and magnesium inside COF nanofiltration membranes

Decai Liao, Zhaoqin Xu, Mingjie Wei and Yong Wang

State Key Laboratory of Materials-Oriented Chemical Engineering, College of Chemical Engineering, Nanjing Tech University, Nanjing, People's Republic of China

ABSTRACT

Membrane technology is playing an important role in the separation of magnesium and lithium from brines, and high Li/Mg selectivity in membrane separation is constantly pursued. However, it has been found that there is always a selectivity variation when using individual salts to replace the salt mixture as the feed, implying that the interference mechanism of mixed cations remains unclear. Herein, by using covalent organic frameworks as an example, we investigate the ion transport behaviours through nanopores with the mixed and individual feeding of LiCl and MgCl₂ via molecular dynamics simulations. There is an evident reduced Li/Mg selectivity while the mixed-salt feed is applied. It is revealed that Li⁺ interacts strongly with pore-wall atoms while Mg²⁺ with water molecules. Consequently, Mg²⁺ tends to flow with water molecules while Li⁺ is prone to adsorb to the pore wall. The presence of Mg²⁺ inside nanopores will bring down water flux and seriously reduce the transport of Li⁺ inside nanopores. The advantage of pre-adsorbing for Li⁺, which promotes the Li/Mg selectivity, is completely balanced out, thus reducing selectivity. Our results also suggest that impeding the entrance of Mg²⁺ into membranes will avoid the selectivity drop not only because of the sieving effecting.

ARTICLE HISTORY

Received 28 March 2022
Accepted 22 June 2022

KEYWORDS

Covalent organic frameworks; Li/Mg separation; nonequilibrium molecular dynamics; nanofiltration; transport mechanism

1. Introduction

The need for grid-scale battery storage is rapidly growing as increasing amounts of renewable energy come online [1]. Together with the exponentially growing demand for portable equipment [2] and electric vehicles [3], thousands of cells are required to transform lithium and electrons into enough energy. Minerals and brines are mainly two resources of lithium, in which more than 60% of lithium resources occur in the aqueous solutions involving salt-lake brines and seawater [4]. According to the recent statistics of the production of lithium, the contribution of brine is nearly two times than that of minerals [5].

Except for some lithium-rich salt lakes in Chile [6], the Mg/Li ratios are higher than 30 in most salt lakes. The success of exploitations from brine in Chile cannot be easily duplicated into other salt lakes due to the high Mg/Li ratios [7], as the cost of chemicals and waste discharge is not affordable if the existing commercial process is applied in such high-Mg/Li-ratio brines [8]. It will be a promising strategy to reduce the Mg/Li ratio rather than directly separating magnesium and lithium by the membrane separation technology. Furthermore, the growing demand for lithium production cannot be satisfied by the slow rate of lithium enrichment by solar evaporation. The membrane-based processes can be applied to selectively enrich/extract the lithium from brines in less time [9].

Up to now, there are a number of reported works on the preparation of nanofiltration (NF) membranes for Mg/Li

separation [10–12]. Most of them are focused on the promotion of Li/Mg selectivity. In order to investigate the promoting mechanism of Li/Mg selectivity, the individual salt feed solutions are usually applied. However, it is observed that the Li/Mg selectivity will change when the mixed-salt solutions are replaced by the individual-salt feed solutions, some of which demonstrate that the Li/Mg selectivity will increase [13,14] and some of which observe reduced selectivity [15–17]. Molecular details as well as the underlying mechanism can hardly be experimentally obtained because it is nearly impossible to directly observe the molecular motion in the NF process taking place in the time scale of 10⁻⁹ s and in the spatial scale of sub-2 nm. Therefore, the mechanism of changing selectivity lacks experimental investigation and remains unclear. Moreover, the rejection performance mainly results from two parts: pore-entrance sieving and in-pore transport [18]. These two parts of contributions cannot be experimentally distinguished, which brings the difficulty of investigating the mechanism of ion rejections and Li/Mg selectivity.

Alternatively, non-equilibrium molecular dynamics (NEMD) simulations provide the possibility to observe the molecular motion of NF and to understand the rejection mechanism of ions from the molecular level. Ruan et al. investigated the rejection mechanism of Mg²⁺ and Li⁺ through porous graphene with various diameters [19]. They concluded that the second hydration layer of Mg²⁺ and Li⁺ will dominate the entrance process of those ions. They subsequently

modified the pore wall of nanopores with hydroxyl or carboxyl groups and found that the interactions of the polar groups with Mg^{2+} are stronger than with Li^+ and the selectivity of Li/Mg is reduced by such modifications [20]. Li et al. investigated the motions of hydrated Mg^{2+} and Li^+ by applying the external electric field in their NEMD simulations and found that the presence of an external electric field will drive the cations and anions to form clusters. Such ion clusters are much larger than the single hydrated ions and consequently are prevented by the pore mouth [21]. Xu et al. charged the surface of membranes to prevent the ions from entering the membranes, and found that moderate surface charging can enhance the Li/Mg selectivity as the electrical repulsion effect is prominent for bivalent Mg^{2+} . However, Mg^{2+} and Li^+ will be both fully rejected if the surface charge is further raised [22].

Most previous works attribute the rejection of Mg^{2+} by the pore mouth to the enhancement of Li/Mg selectivity. However, those findings cannot explain the mechanism of selectivity variation for the cases using salt mixtures as the feed solution. Moreover, the above-mentioned works used two-dimensional monolayers as the membrane, which only considers the membrane entrance process and does not allow investigations on the transport of ions inside the membrane. Since hydrated Mg^{2+} and Li^+ have highly closing diameters (0.99 vs. 1.05 nm, Figure S3), the pore mouth sieving of these two types of cations requires membranes with sub-angstrom-level tunable pore sizes which are extremely difficult to be experimentally realised. Therefore, the presence of both Mg^{2+} and Li^+ inside membranes is inevitable. Our previous works [18,23] indicate that the in-pore transport of ions plays an important role in the rejection of ions and consequently influences the selectivity in the salt mixture cases. It is worthy of investigating the effect of in-pore transport of Mg^{2+} and Li^+ as the understanding of the transport mechanism would help to design advanced membranes for improved Li/Mg selectivity. Since most NF membranes are composed of polymers, it is better to model the membrane with polymers of disordered pore structure. However, such a disordered structure will bring more difficulties to identify the influence of pore size and dehydration degrees of ions. Carbon nanotubes are usually utilised to model membranes, however, they are distinct from polymers in chemistry. Fortunately, covalent organic frameworks (COFs) are polymers that have a uniform pore structure, which is ideal for modelling the NF membranes. Moreover, there are several efforts to prepare NF membranes with COFs [24,25], therefore, it is worthy to investigate the separation mechanism of Li/Mg by COFs NF membranes.

In this work, we select an imine-linked, stable covalent organic framework (COF), TpPa (synthesised by 1,3,5-triformylphloroglucinol and p-phenylenediamine) [26], with various numbers of monolayers to build up the membranes. The pore size of TpPa is 1.58 nm, so that the contributions of pore-mouth sieving and in-pore transport effects can be both investigated. The feed solutions of individual-salt LiCl or MgCl_2 , as well as mixed-salt LiCl and MgCl_2 are separately set up. NEMD simulations with pressure drop as driving force are applied to simulate the pressure-driven NF processes. After finishing the simulations, the rejections of two cations are firstly obtained, in which the reduced Li/Mg selectivity is

discovered while the feed solutions are replaced from individual to mixed salts. From the analysis of the rejection mechanism based on the separate two factors, namely pore-entrance sieving and in-pore transport, it is impossible to explain the dropping selectivity. By establishing the equation of describing the relationship of Li/Mg selectivity, the mechanism of reduced selectivity, as well as its origin at the molecular level, is clearly revealed. Also importantly, the results obtained in this work warn us that selectivity mechanism analysis determined in the lab by comparing the rejection to individual Li and Mg may not reliably represent the ‘true selectivity’ in real-world applications in which Li and Mg are simultaneously present in the feed. The interference effect should not be ignored.

2. Models and methods

2.1. Construction of models

The multilayered TpPa, which is well introduced in our previous work [26,27], is selected to act as the membranes because it has the chemical structure close to commercial polyamide NF membranes. At the same time, its uniform morphological frame provides an opportunity to hold the pore structure-related parameters, with which the relationship of molecular properties can be easily quantified. Moreover, the pore size of TpPa (1.58 nm) is also near to that of most commercial NF membranes. Therefore, the findings obtained from TpPa membranes should also be valid to polyamide NF membranes, and are expected to be helpful in the development of advanced NF membranes with high Mg/Li selectivity. Moreover, the main purpose of this work is investigating the whole transport process, including the in-pore transport, therefore, the entering of two types of cations should not be completely avoided. The pore size of TpPa is proper for the hydrated cations as they could permeate into TpPa nanopores while there is dehydration process of these cations.

The atomic structure of TpPa used in this work is obtained from the CoRE COF database [28], which contains many structures constructed from experimental characterisations [29–31]. Multilayered TpPa is selected in this work to perform simulations, the effective aperture of these structures is 1.58 nm. More details on constructing the molecular model of TpPa membranes are described in our previous work [26].

Two reservoirs are then placed on each side of the membrane that serve as feed side and permeate side, respectively (Figure 1). The concentration of the individual-salt system ($\text{LiCl} + \text{H}_2\text{O}$ or $\text{MgCl}_2 + \text{H}_2\text{O}$) is 0.98 mol L^{-1} . For the mixed-salt system ($\text{LiCl} + \text{MgCl}_2 + \text{H}_2\text{O}$) with Li/Mg ratio is 1:1 (molar ratio, denoted as $X_{\text{Li}/\text{Mg}} = 1:1$), the concentrations of LiCl and MgCl_2 are both 0.5 mol L^{-1} . For the cases of $X_{\text{Li}/\text{Mg}} = 1:4$, the solution is the mixed solution of 0.2-mol L^{-1} LiCl and 0.8-mol L^{-1} MgCl_2 .

2.2. Simulation details

The interactions of all atoms include the Lennard-Jones (L-J) van der Waals (VDW) and the Columbic potentials. The SPC/E model is selected for water molecules and The Dreiding

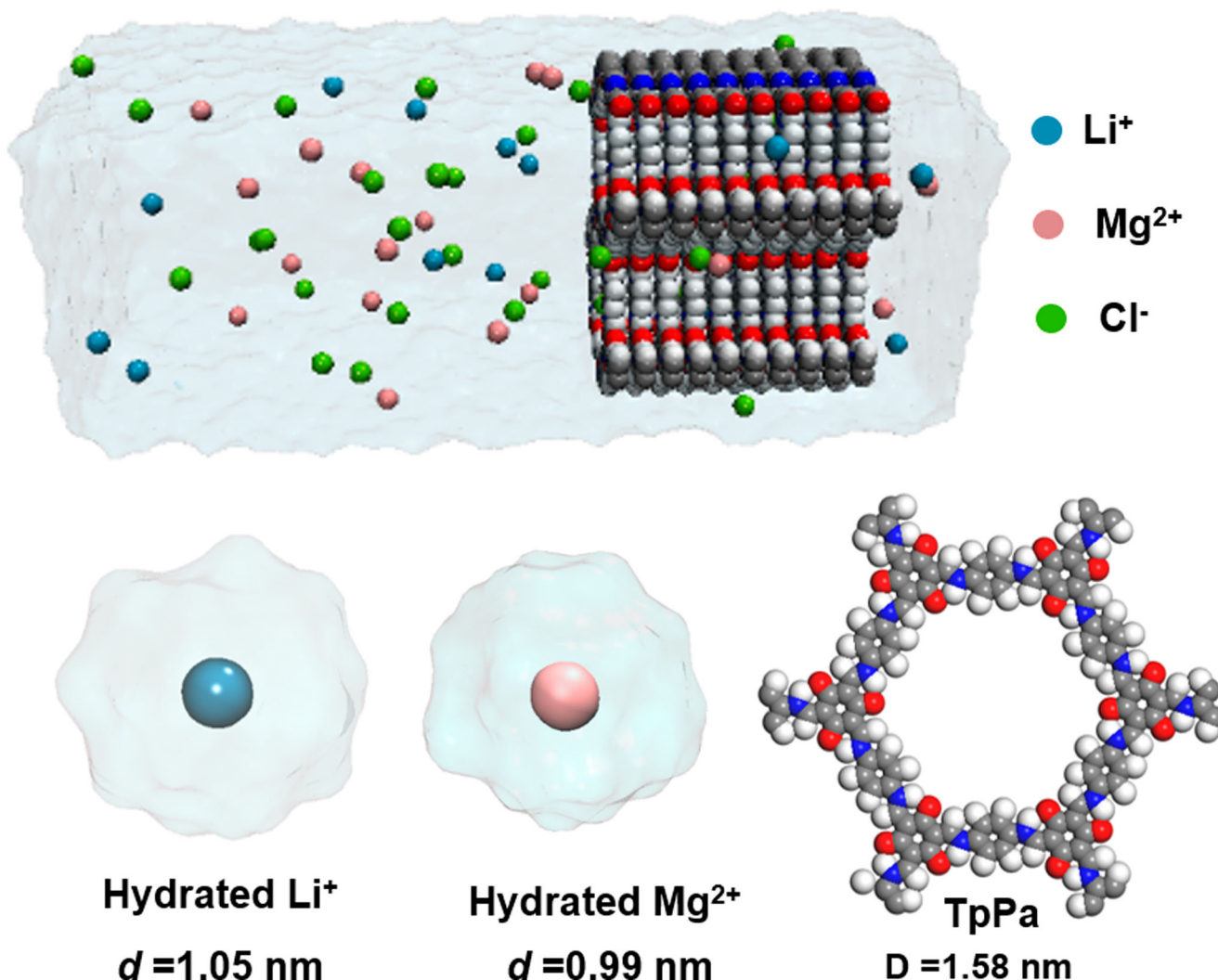


Figure 1. (Colour online) (a) molecular model of simulations and (b) hydrated Li⁺, (c) hydrated Mg²⁺ and (d) pore structure of TpPa.

force field [32] are applied for TpPa atoms, which are usually adopted in most COFs-based simulations [28,33,34]. The interaction parameters of ions are referred to the optimised parameters [35,36]. Lorentz-Berthelot mixing rule is applied for all pair-wise VDW terms. Density functional theory of the grid-based ChelpG algorithm is performed to obtain electrostatic potential charges, which are employed as atomic partial charges [34].

All simulations are performed using the large-scale atomic/molecular massively parallel simulator (LAMMPS). The cutoff distances of L-J and Columbic potentials are set to 1.0 and 1.2 nm, respectively. The accuracy of particle-particle particle-mesh for computing long-range electrostatic interactions is 10^{-5} . A pump method is selected to drive the flow in this work [18]. For every simulation case, we first perform an energy minimisation with a tolerance of 10^{-5} , then pre-equilibration is performed so as to ensure that the pore is saturated with water molecules and the ions reach adsorption equilibrium inside the nanopores.

After that, NEMD simulations are performed at 300 K. The pressure drop (ΔP) is set to 200 MPa, which is much higher than the experimental values, because a large ΔP helps to

keep a high signal-to-noise ratio and save simulation time, which has been extensively used [37–39]. External forces are applied to the atoms in selected region. The ΔP is described as,

$$\Delta P = \frac{n_{\text{ion}}f_{\text{ion}} + n_{\text{water}}f_{\text{water}}}{A} \quad (1a)$$

$$\frac{f_{\text{ion}}}{m_{\text{ion}}} = \frac{f_{\text{water}}}{m_{\text{water}}} \quad (1b)$$

where n is the number of species in the selected region, f is the external force, A is the selected area; m is the molecular mass of species. Equation 1(b) indicates that we apply the same acceleration for each atom in the selected region. The region selected to apply acceleration is located at the left edge of feed size, which is 0.5 nm wide.

Each simulation case runs for 40–50 ns with a time step of 1 fs. After the systems reach a steady state, we update the trajectory file every 1 ps which is used for further analysis. The ion rejection is calculated as,

$$R = 1 - \frac{C_{\text{permeate}}}{C_{\text{feed}}} \quad (2)$$

where C_{permeate} and C_{feed} denote the concentration of permeate

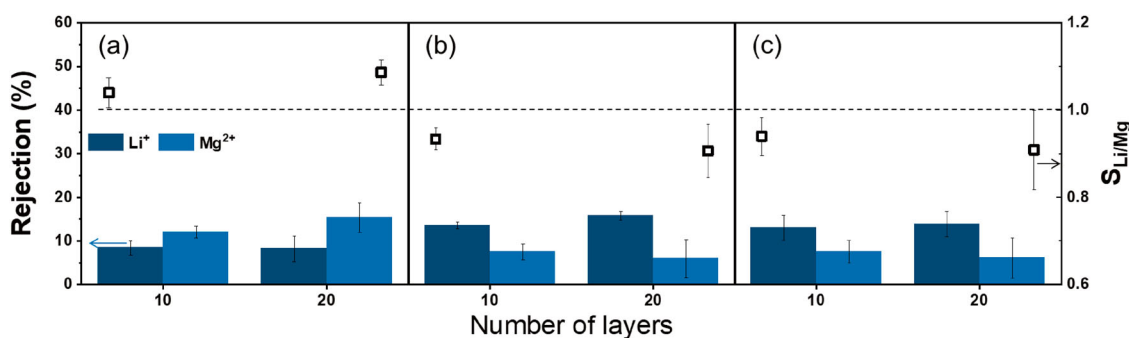


Figure 2. (Colour online) Ion rejections and Li/Mg selectivities of TpPa membranes for the cases of (a) individual-salt solution, (b) mixed-salt solution of $X_{\text{Li/Mg}} = 1:1$, (c) mixed-salt solution of $X_{\text{Li/Mg}} = 1:4$. The dash line indicates the value of selectivity being 1.

side and feed side, respectively. No clear boundary exists between the feed and permeate side because of the existence of periodical boundary conditions. Therefore, the rejection can be calculated by [40,41]

$$R = 1 - \frac{F_i}{n_i} / \frac{F_w}{n_w} \quad (3)$$

where the F_i and F_w are the fluxes of ions and water molecules, respectively, while n_i is the number of ions in the simulation box, and n_w is that of water molecules.

3. Results and discussions

3.1. The apparent ion rejection

Since the selectivity of membranes for Li^+ over Mg^{2+} is defined by the rejection results of these two types of cations as,

$$S_{\text{Li/Mg}} = \frac{C_{\text{Li,p}}/C_{\text{Mg,p}}}{C_{\text{Li,f}}/C_{\text{Mg,f}}} = (1 - R_{\text{Li}})/(1 - R_{\text{Mg}}) \quad (4)$$

it is necessary to present the apparent rejection results of Li^+ and Mg^{2+} . For the cases of individual salt (shown in Figure 2 (a)), the rejections of Li^+ and Mg^{2+} are close regardless of the number of COF monolayers. As indicated in our previous work [42], the rejection will not change while the membrane thickness reaches and gets larger than the diameter of hydrated ions. In this work, the thickness of 10-layered TpPa membranes is 3.22 nm, which is much larger than the diameter of all hydrated ions in this work, consequently the rejection of ions is almost independent of the membrane thickness as shown in Figure 2. Since the selectivity is calculated based on the rejection results of ions, it is independent of the membrane thickness as well.

In Figure 2(a), the selectivity keeps around 1.1, indicating that such membranes are permselective to Li^+ rather than Mg^{2+} , or that Li^+ can pass through TpPa membranes more easily and rapidly than Mg^{2+} . For mixed-salt cases of $X_{\text{Li/Mg}} = 1:1$ (Figure 2(b)), the rejection of Li^+ is surprisingly higher than that of Mg^{2+} . Therefore, the selectivity of membranes for Li^+ over Mg^{2+} is reducing compared to the individual-salt cases. When the molar ratio is tuned to 1:4 (Figure 2(c)), the selectivity remains at around 0.9, confirming that there is reduced selectivity when two types of cations are mixed, which is also observed in experiments of similar conditions

[17], that is the concentration of feed solution is the same for individual- or mixed-salt cases.

The transport numbers of cations and fluxes of water are then calculated because the apparent rejection is highly dependent on water flux, according to Equation (3). As shown in Figure 3(a–c), the transport numbers of Li^+ are obviously higher than those of Mg^{2+} for the cases of individual salts. When two types of salts are mixed, the ion fluxes all drop much. Compared to the drop degree for Mg^{2+} , the transport numbers of Li^+ decline even more. Consequently, the fluxes of Li^+ are lower than those of Mg^{2+} , which are in accordance with rejection results and confirm the existence of reduced selectivity.

3.2. The contribution of pore-entrance sieving effect

In order to further understand the mechanism behind the phenomenon of reduced selectivity, we take the rejection mechanism of Li^+ and Mg^{2+} into consideration. In our previous work, the contribution of rejection can be divided into two parts,

$$R = 1 - \frac{c_{\text{in}}}{c_0} \cdot \frac{\nu_i}{\nu_w} \quad (5)$$

where c_{in}/c_0 is the concentration ratio of the in-pore ions and outside those, which represents the pore-entrance-sieving effect. Higher values of c_{in}/c_0 will result in lower rejection rates, which indicates a weaker pore-entrance-sieving effect. ν_i/ν_w is the ratio of ion flow rates to water those inside nanopores, and this part can be recognised as the in-pore-transport effect. Larger values of ν_i/ν_w suggest less pronounced in-pore-transport effects as it will cause lower rejection rates.

The contribution of the pore-entrance-sieving effect (c_{in}/c_0) is first considered. As shown in Figure 4, the c_{in}/c_0 values of Li^+ for all cases are higher than those of Mg^{2+} , indicating the weaker pore-entrance-sieving effect for Li^+ . These results can be accounted that Li^+ are more favourable to get into TpPa nanopores. In order to figure out the reason behind, we turn to focus on the structure of hydration shell when these two types of cations are inside TpPa nanopores.

Since the cations are hydrated in the aqueous solutions, the change of hydration numbers when they try to enter the nanopores will significantly influence the possibility of entrance. Similar to our previous work [43], we calculated the

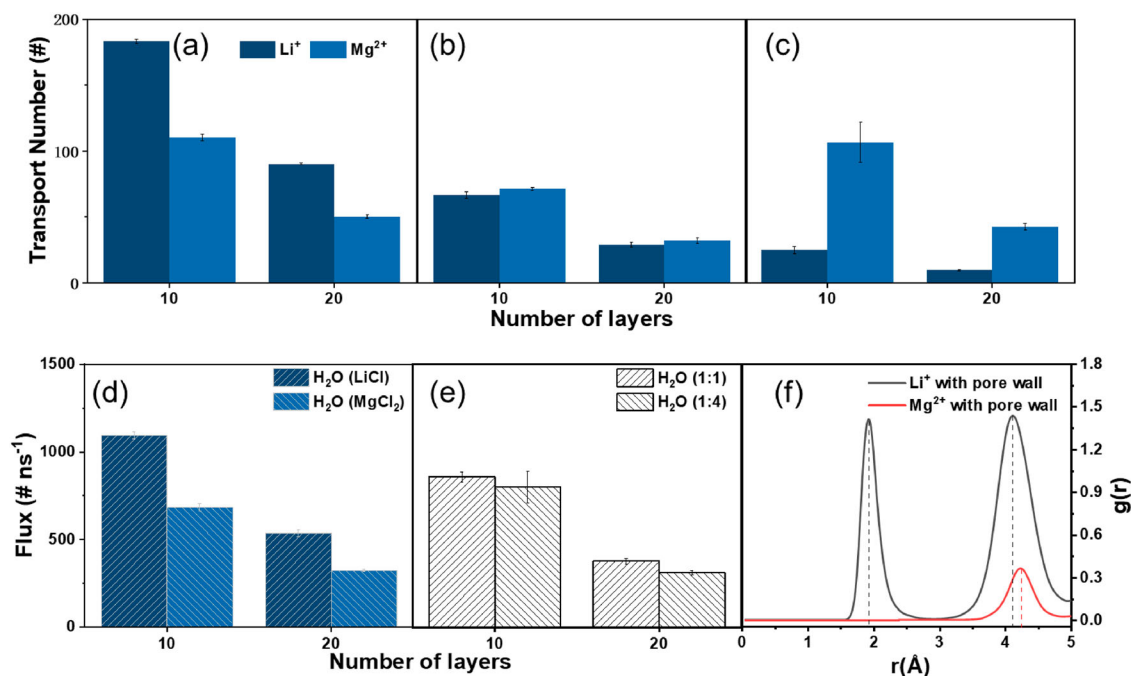


Figure 3. (Colour online) Ion transport numbers of Li⁺ and Mg²⁺ for the cases of (a) individual-salt solution, (b) mixed-salt solution of $X_{\text{Li}/\text{Mg}} = 1:1$ (c) mixed-salt solution of $X_{\text{Li}/\text{Mg}} = 1:4$; water flux of (d) individual-salt solution (e) mixed-salt solution and (f) RDF for Li⁺ and Mg²⁺ with pore-wall atoms

dehydration degree (η_d) of these two types of cations inside TpPa nanopores as,

$$\eta_d = 1 - \frac{n_{in}}{n_0} \quad (6)$$

where n_{in} is the minimum number of water molecules inside ion-hydration shells when they are inside nanopores; n_0 is the average number of water molecules inside the hydration shells of ions when they are in the bulk aqueous solutions.

From Figure 5, it is obvious that the values of η_d for Li⁺ are all higher than those of Mg²⁺, indicating the higher dehydration degree for Li⁺. Such phenomena can be interpreted as hydrated Li⁺ are softer balls compared to those of Mg²⁺, due to the monovalent of Li⁺ has a weaker attraction to hold water molecules around them. When cations try to enter TpPa nanopores, it is easier for Li⁺ to peel off some water molecules in their hydration shell and then move into the nanopores.

It is puzzled that the diameters of hydrated Li⁺ and Mg²⁺ are no more than 1.05 nm while the effective diameter of TpPa nanopores is 1.58 nm, illustrating the needless for cations to peel off their hydration shells. The hydrophilicity of TpPa results in a hydration shell around pore walls [26], thus the pre-occupying water molecules around pore walls consequently reduced the effective diameter of TpPa for cations. When water molecules pass through such nanopores, the water molecules around the pore wall can exchange with those in the central of nanopores, thus will not significantly influence the entrance of water molecules as well as their transport through the nanopores. However, when hydrated cations reach the pore mouth, the water molecules in the hydration shell of cations cannot easily exchange with those in pore wall shells. Such an exchange process is certainly related to the dehydration degree of cations. If the hydration shell is rigid (e.g. Mg²⁺), the possibility of exchange is lower, therefore, it is more difficult for cations with rigid hydration shells to enter the nanopores.

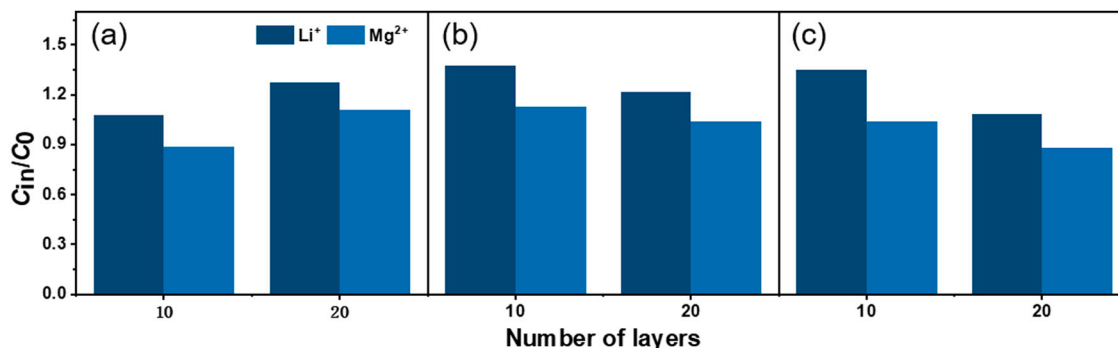


Figure 4. (Colour online) Values of c_{in}/c_0 in multilayered TpPa membranes for the cases of (a) individual-salt solution, (b) mixed-salt solution of $X_{\text{Li}/\text{Mg}} = 1:1$, (c) mixed-salt solution of $X_{\text{Li}/\text{Mg}} = 1:4$

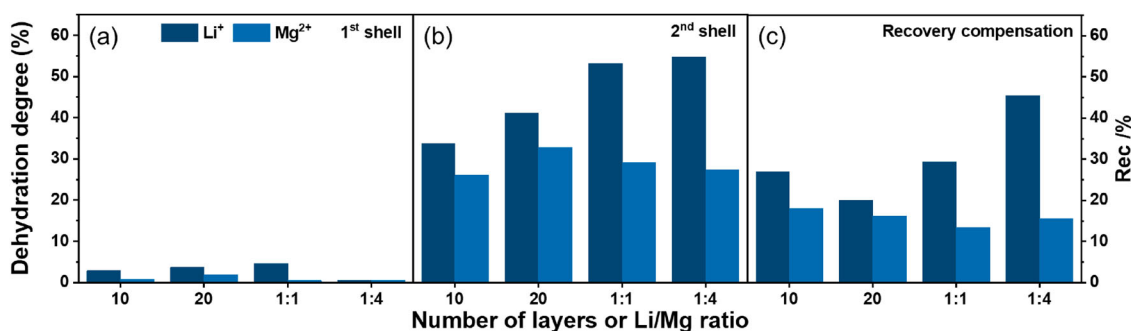


Figure 5. (Colour online) Dehydration degree and hydration recovery rate results: (a) dehydration degree of 1st shell on cations; (b) dehydration degree of 2nd shell on cations; (c) hydration recovery rate due to the pore wall compensation

Moreover, the polar atoms at pore walls will also be involved with the hydration shell of cations [18], therefore, we calculate the radial distribution function ($g(r)$) of cations with oxygen atoms on pore walls (shown in Figure 3(f)) to investigate the influence of pore-wall atoms. There are two peaks for Li⁺, indicating that the pore-wall atoms are involved in the first and second shells of hydrated Li⁺. The only one peak for Mg²⁺ at r of 0.42 nm represents the pore-wall atoms being only involved in the second shell of hydrated Mg²⁺. Moreover, the height of the two peaks for Li⁺ is obviously large compared to the one for Mg²⁺. Higher peaks or larger peak area represents more pore-wall atoms involved in the hydration shell of cations. As discussed in our previous work [18], the involved pore-wall atoms will help the hydrated cations to enter the nanopores because the dehydration of cations is somehow compensated by the pore-wall atoms.

To quantify the compensation degree of pore-wall atoms on dehydration, the hydration recovery rate (Rec) is calculated, which is defined as

$$\text{Rec} = \frac{n_{PW}}{n_0 - n_{in}} \quad (7)$$

where n_{PW} is the average hydration number of pore-wall atoms

for cations. A higher *Rec* value for Li⁺ represents that the dehydration is compensated in a higher degree by pore-wall atoms, compared to Mg²⁺.

Both the dehydration and compensation results promise the easiness for Li⁺ to enter the TpPa nanopores, which is in accordance with higher values of c_{in}/c_0 in Figure 4. However, all the results above cannot explain the reduced selectivity as the values of Li⁺ are all higher than those of Mg²⁺ no matter of individual- or mixed-salt cases. It is necessary to figure out the other contribution to rejection, such as the in-pore-transport effect.

3.3. The contribution of in-pore transport

The in-pore-transport effect (v_i/v_w) is obtained from calculating the residence time of water molecules and ions inside nanopores (shown in Figure 6), as the velocity can be easily calculated by dividing the membrane thickness by the residence time. From Figure 6, we observe that the values of residence time for Li⁺ are shorter than those for Mg²⁺, predicting the weaker interaction of Li⁺ with pore-wall atoms. However, the results in the above section predict that the hydrated Li⁺ has a stronger interaction with pore-wall atoms, which is

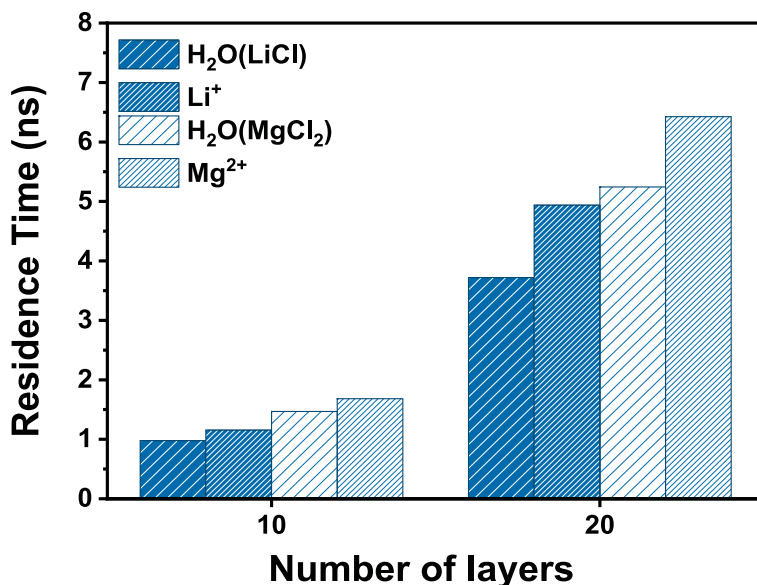


Figure 6. (Colour online) Residence time of cations and water molecules inside TpPa nanopores for the cases of individual salts.

Table 1. Values of v_i/v_w for all cases.

Cases	Individual salt		$X_{Li/Mg} = 1:1$		$X_{Li/Mg} = 1:4$	
	10 layers	20 layers	10 layers	20 layers	10 layers	20 layers
	v_{Li}/v_w	0.849	0.753	0.738	0.689	0.715
v_{Mg}/v_w	0.873	0.775	0.975	0.919	0.907	0.858

contradictory to the results of residence time. If we further compare the residence time of water in two distinct individual-salt cases. The residence time of water in Li^+ cases is evidently shorter than that in Mg^{2+} cases. Moreover, the residence time of water in Mg^{2+} cases (3rd column in Figure 6) is longer than that of Li^+ (2nd column in Figure 6). Since the v_i/v_w rather than v_i represents the effect of in-pore transport, the values of v_i/v_w are calculated and listed in Table 1.

For the individual-salt cases of the same membrane thickness, the values of v_{Li}/v_w and v_{Mg}/v_w are close, indicating that relative transport rates (compared to water molecules) are almost the same for both two types of cations. While two types of cations are mixed, the values of v_{Li}/v_w are much lower than those of v_{Mg}/v_w . These are in accordance with the results of hydration compensation in the above section, that the interaction of Li^+ with pore-wall atoms is stronger and thus Li^+ has lower transport velocity. From Table 1, the values of v_{Mg}/v_w are all larger than those of v_{Li}/v_w no matter of individual- or mixed-salt cases. Therefore, it is impossible to figure out the mechanism of reduced selectivity by separately analyzing the contributions of pore-entrance sieving and in-pore-transport effects. Moreover, the strong interaction of Li^+ with pore wall is harmful to the in-pore transport but favourable for the contribution of c_{in}/c_0 at the same time. Therefore, it is necessary to consider these two contributions at the same time.

3.4. Analysis of reduced-selectivity mechanism

From Equations (4) and (5), we can obtain the relationship between selectivity and two contributions of rejection as,

$$S_{Li/Mg} = \left(\frac{c_{in,Li}}{c_{in,Mg}} / \frac{c_0,Li}{c_0,Mg} \right) \cdot \left(\frac{v_{Li}}{v_{Mg}} / \frac{v_w,Li}{v_w,Mg} \right) = \phi_c \cdot \phi_v \quad (8)$$

The calculated S are listed in Table 2. From Table 2, the reduced selectivity is evidently present, as the values of S are larger than 1 for individual-salt cases but lower than 1 for mixed-salt those.

Furthermore, in order to figure out the mechanism of reduced selectivity, we separate the selectivity into two parts as contributions of ion concentration and transport, which are denoted by ϕ_c and ϕ_v , respectively. The values are calculated for all cases and listed in Table 2 as well. It is evident that the contribution of ion concentration (ϕ_c) maintains at

Table 2. Values of ϕ_c , ϕ_v and calculated $S_{Li/Mg}$ for all cases.

Cases	Individual salt		$X_{Li/Mg} = 1:1$		$X_{Li/Mg} = 1:4$	
	10 layers	20 layers	10 layers	20 layers	10 layers	20 layers
	ϕ_c	1.211	1.148	1.214	1.214	1.247
ϕ_v	0.973	0.972	0.757	0.750	0.788	0.780
$S_{Li/Mg}$	1.178	1.116	0.919	0.911	0.982	0.870

Table 3. Self-diffusion coefficients (D , $10^{-9} \text{ m}^2 \text{ s}^{-1}$) of cations in bulk solution.

	Li^+ (LiCl)	Li^+ (1:1)	Li^+ (1:4)	Mg^{2+} ($MgCl_2$)	Mg^{2+} (1:1)	Mg^{2+} (1:4)
D	0.332	0.184	0.293	0.175	0.085	0.092

around 1.2 no matter of the individual- or mixed-salt cases. However, the contribution of transport (ϕ_v) for individual-salt cases is close to 1 but is no more than 0.8 for mixed-salt cases. $v_w,Li/v_w,Mg$ equals 1 for the mixed-salt cases because there is only one water flux. However, for the individual-salt cases, $v_w,Li/v_w,Mg$ is obviously lower than 1. The reduced selectivity might result from the water fluxes for distinct individual-salt cases.

From Figure 6, the residence time of water inside TpPa membranes is longer for individual- $MgCl_2$ cases. Moreover, the permeance of water ($1154 \text{ L m}^{-2} \text{ h}^{-1} \text{ bar}^{-1}$) is much reduced compared to that of pure water cases ($3736 \text{ L m}^{-2} \text{ h}^{-1} \text{ bar}^{-1}$) [26]. Furthermore, the water permeances of mixed cases (Figure 3(e)) are close to those of individual- $MgCl_2$ (Figure 3(d)). It is very possible that the existence of Mg^{2+} inside TpPa membranes will significantly reduce the water permeability. In the cases of individual- $LiCl$ (Figure 3(d)), the water permeability is slightly reduced compared to pure water permeance, because the hydration shell of Li^+ is soft and water molecules can easily exchange during they pass through TpPa nanopores. Therefore, the water molecules will not be significantly hindered when the Li^+ exists inside TpPa nanopores.

Moreover, the self-diffusion coefficients of Li^+ and Mg^{2+} in bulk water are calculated based on the mean square displacement results (shown in Figure S1) and are listed in Table 3. The self-diffusion coefficients of Li^+ are higher than those of Mg^{2+} , indicating that the Li^+ will move freely rather than follow the water molecules when the solution is in the state of flow. In other words, the Mg^{2+} tend to follow the water flow while Li^+ will not. Together with the understanding of stronger interaction of Li^+ with pore wall, it can be concluded that, during the process of cations passing through the TpPa nanopores, Li^+ would like to interact with pore wall rather than flow with water, on the other side, the Mg^{2+} will follow the water molecules to pass through the TpPa nanopores. The results of $v_w,Li/v_w,Mg$ can also confirm this conclusion.

When the ions transport through nanopores, there is mainly one driving force and one dragging force. The driving force comes from the water flow while the dragging force originates from the interaction of ions with pore wall atoms. For the mixed-salt cases, the presence of Mg^{2+} inside TpPa nanopores will reduce the water flux, the driving forces, while the water permeability is determined by the Mg^{2+} (similar to the individual $MgCl_2$ cases). As discussed above, the Mg^{2+} will follow the water flow although the flow rate is reduced. However, the Li^+ prefer to interacting with pore walls rather than flow with water. The driving force is reduced but dragging force remains, resulting in a further reduction of Li^+ flux. If the membrane thickness is enlarged, such reduction effect will be promoted as the permeance of Li will encounter more high energy barriers while Mg^{2+} will not (shown in Figure S2).

4. Conclusions

In order to uncover the reason for the variation of Li/Mg selectivity when the feed solution is replaced from mixed salts to individual salt, we perform a series of NEMD simulations of Li^+ and Mg^{2+} transport through multilayered TpPa membranes with individual- or mixed-salt feed solutions. The rejection performance for Li^+ and Mg^{2+} as well as Li/Mg selectivity are firstly investigated. It is evident that the Li/Mg selectivity drops from ~ 1.1 to ~ 0.9 while two types of salts are mixed in the feed solution. Moreover, the selectivity is surprisingly reduced, indicating the membrane prefers to permeate Mg^{2+} rather than Li^+ in the mixed-salt condition, which is opposite to the result of the individual-salt condition. The analysis of both pore-entrance-sieving effects as well as the in-pore-transport effects indicates that Li^+ has a stronger interaction with pore-wall atoms resulting in the convenience of Li^+ to enter nanopores but lower transport ability inside them. However, the separate analysis of these two contributions cannot explain the phenomenon of reduced selectivity. By coupling the influence of them, we conclude that the reduced selectivity mainly originates from the reduced water flux in mixed-salt cases, which is due to the presence of Mg^{2+} inside nanopores. The molecular characterisations also reveal that Mg^{2+} prefers to flow with water while Li^+ is more likely to adsorb onto the pore walls. Therefore, the reduced water flux, or the driving force, plays a distinctly negative role in the transport of Li^+ but rarely in that of Mg^{2+} . The flux of Mg^{2+} is then evidently larger than the one of Li^+ in the mixed-salt cases, leading to the selective permeate of Mg^{2+} , which is opposite to the results in the individual-salt cases. The findings in this work reveal the mechanism of the reduced Li/Mg selectivity in experiments when mixed-salt feed solution is applied. It could be deduced that impeding the entrance of Mg^{2+} into membranes might avoid the selectivity drop in experiments, not only because of the pore-entrance sieving effect. This conclusion is still valid if the membranes are thick enough, i.e. thicker than 3.0 nm, as the mechanism is the same for the cases with distinct membrane thickness in this work. The interference effect of cations, especially its influence on the transport of cations inside membranes should not be ignored, which is helpful for the design of high-performance NF membranes for Li/Mg separation.

Acknowledgements

The authors thank the High Performance Computing Centre of Nanjing Tech University for supporting the computational resources.

Disclosure statement

No potential conflict of interest was reported by the author(s).

Funding

This work was supported by the Natural Science Foundation of Jiangsu Province [grant number BK20190085], and the National Natural Science Fund for Distinguish Young Scholars [grant number 21825803].

References

- Service RF. Zinc aims to beat lithium batteries at storing energy. *Science*. 2021;372(6545):890–891.
- Tarascon JM, Armand M. Issues and challenges facing rechargeable lithium batteries. *Nature*. 2001;414(6861):359–367.
- Morse I. A dead battery dilemma. *Science*. 2021 May 21;372(6544):780–783.
- Zhang Y, Sun W, Xu R, et al. Lithium extraction from water lithium resources through green electrochemical-battery approaches: a comprehensive review. *J Clean Product*. 2021;285:124905.
- Choubey PK, Kim M-S, Srivastava RR, et al. Advance review on the exploitation of the prominent energy-storage element: lithium. Part I: from mineral and brine resources. *Miner Eng*. 2016;89:119–137.
- Cabello J. Lithium brine production, reserves, resources and exploration in Chile: an updated review. *Ore Geol Rev*. 2021;128:103883.
- Swain B. Recovery and recycling of lithium: a review. *Sep Purif Technol*. 2017;172:388–403.
- Kelly JC, Wang M, Dai Q, et al. Energy, greenhouse gas, and water life cycle analysis of lithium carbonate and lithium hydroxide monohydrate from brine and ore resources and their use in lithium ion battery cathodes and lithium ion batteries. *Resour Conserv Recycl*. 2021;174:105762.
- Somrani A, Hamzaoui AH, Pontie M. Study on lithium separation from salt lake brines by nanofiltration (NF) and low pressure reverse osmosis (LPRO). *Desalination*. 2013;317:184–192.
- Xu S, Song J, Bi Q, et al. Extraction of lithium from Chinese salt-lake brines by membranes: design and practice. *J Membr Sci*. 2021;635:119441.
- Zhang Y, Wang L, Sun W, et al. Membrane technologies for Li⁺/Mg²⁺ separation from salt-lake brines and seawater: a comprehensive review. *J Indus Eng Chem*. 2020;81:7–23.
- Li X, Mo Y, Qing W, et al. Membrane-based technologies for lithium recovery from water lithium resources: a review. *J Membr Sci*. 2019;591:117317.
- Wu H, Lin Y, Feng W, et al. A novel nanofiltration membrane with [MimAP][Tf2N] ionic liquid for utilization of lithium from brines with high Mg²⁺/Li⁺ ratio. *J Membr Sci*. 2020;603:117997.
- Awais Ashraf M, Li X, Wang J, et al. DiaNanofiltration-based process for effective separation of Li⁺ from the high Mg²⁺/Li⁺ ratio aqueous solution. *Sep Purif Technol*. 2020;247:116965.
- Yang Z, Fang W, Wang Z, et al. Dual-skin layer nanofiltration membranes for highly selective Li⁺/Mg²⁺ separation. *J Membr Sci*. 2021;620:118862.
- Lu Z, Wu Y, Ding L, et al. A lamellar MXene (Ti₃C₂Tx)/PSS composite membrane for fast and selective lithium-ion separation. *Angewand Chem Int Ed*. 2021;60(41):22265–22269.
- Xu P, Wang W, Qian X, et al. Positive charged PEI-TMC composite nanofiltration membrane for separation of Li⁺ and Mg²⁺ from brine with high Mg²⁺/Li⁺ ratio. *Desalination*. 2019;449:57–68.
- Xu F, Wei M, Zhang X, et al. Ion rejection in covalent organic frameworks: revealing the overlooked effect of in-pore transport. *ACS Appl Mater Interfaces*. 2019;11(48):45246–45255.
- Ruan Y, Zhu Y, Zhang Y, et al. Molecular dynamics study of Mg²⁺/Li⁺ separation via biomimetic graphene-based nanopores: the role of dehydration in second shell. *Langmuir*. 2016;32(51):13778–13786.
- Zhu Y, Ruan Y, Zhang Y, et al. Mg²⁺-channel-inspired nanopores for Mg²⁺/Li⁺ separation: the effect of coordination on the ionic hydration microstructures. *Langmuir*. 2017;33(36):9201–9210.
- Li Y, Yue X, Huang G, et al. Li⁺ selectivity of carboxylate graphene nanopores inspired by electric field and nanoconfinement. *Small*. 2021. 2006704. DOI:10.1002/smll.202006704.
- Xu F, Dai L, Wu Y, et al. Li⁺/Mg²⁺ separation by membrane separation: the role of the compensatory effect. *J Membr Sci*. 2021;636:119542.
- Xu F, Wei M, Zhang X, et al. Effect of hydrophilicity on water transport through sub-nanometer pores. *J Membr Sci*. 2020;611:118297.
- Li Y, Wu Q, Guo X, et al. Laminated self-standing covalent organic framework membrane with uniformly distributed subnanopores for ionic and molecular sieving. *Nat Commun*. 2020;11(1):599.

- [25] Yuan S, Li X, Zhu J, et al. Covalent organic frameworks for membrane separation. *Chem Soc Rev*. 2019;48(10):2665–2681.
- [26] Zhou W, Wei M, Zhang X, et al. Fast desalination by multilayered covalent organic framework (COF) nanosheets. *ACS Appl Mater Interfaces*. 2019;11(18):16847–16854.
- [27] Wang R, Shi XS, Zhang Z, et al. Unidirectional diffusion synthesis of covalent organic frameworks (COFs) on polymeric substrates for dye separation. *J Membr Sci*. 2019 Sep;586:274–280.
- [28] Tong MM, Lan YS, Yang QY, et al. Exploring the structure-property relationships of covalent organic frameworks for noble gas separations. *Chem Eng Sci*. 2017;168:456–464.
- [29] Stegbauer L, Hahn MW, Jentys A, et al. Tunable water and CO₂ sorption properties in isostructural azine-based covalent organic frameworks through polarity engineering. *Chem Mater*. 2015;27(23):7874–7881.
- [30] Li ZP, Zhi YF, Feng X, et al. An azine-linked covalent organic framework: synthesis, characterization and efficient gas storage. *Chem Eur J*. 2015;21(34):12079–12084.
- [31] Kang ZX, Peng YW, Qian YH, et al. Mixed matrix membranes (MMMs) comprising exfoliated 2D covalent organic frameworks (COFs) for efficient CO₂ separation. *Chem Mater*. 2016;28(5):1277–1285.
- [32] Mayo SL, Olafson BD, Goddard WA. Dreiding – a generic force-field for molecular simulations. *J Phys Chem*. 1990;94(26):8897–8909.
- [33] Lin LC, Choi JW, Grossman JC. Two-dimensional covalent triazine framework as an ultrathin-film nanoporous membrane for desalination. *Chem Commun*. 2015;51(80):14921–14924.
- [34] Tong MM, Yang QY, Xiao YL, et al. Revealing the structure-property relationship of covalent organic frameworks for CO₂ capture from postcombustion gas: a multi-scale computational study. *Phys Chem Chem Phys*. 2014;16(29):15189–15198.
- [35] Joung IS, Cheatham TE. Determination of alkali and halide monovalent ion parameters for use in explicitly solvated biomolecular simulations. *J Phys Chem B*. 2008;112(30):9020–9041.
- [36] Li P, Roberts BP, Chakravorty DK, et al. Rational design of particle Mesh Ewald compatible Lennard-Jones parameters for +2 metal cations in explicit solvent. *J Chem Theory Comput*. 2013;9(6):2733–2748.
- [37] Chen B, Jiang HF, Liu X, et al. Molecular insight into water desalination across multilayer graphene oxide membranes. *Appl Mater Inter*. 2017;9(27):22826–22836.
- [38] Heiranian M, Farimani AB, Aluru NR. Water desalination with a single-layer MoS₂ nanopore. *Nat Commun*. 2015;6:8616.
- [39] Cohen-Tanugi D, Grossman JC. Water desalination across nanoporous graphene. *Nano Letters*. 2012;12(7):3602–3608.
- [40] Corry B. Designing carbon nanotube membranes for efficient water desalination. *J Phys Chem B*. 2008;112(5):1427–1434.
- [41] Kohler MH, Bordin JR, Barbosa MC. 2D nanoporous membrane for cation removal from water: effects of ionic valence, membrane hydrophobicity, and pore size. *J Chem Phys*. 2018;148:22.
- [42] Zhang X, Wei M, Xu F, et al. Thickness-dependent ion rejection in nanopores. *J Membr Sci*. 2020;601:117899.
- [43] Xu F, Wei M, Wang Y. Effect of hydrophilicity on ion rejection of sub-nanometer pores. *Sep Purif Technol*. 2021;257:117937.